

## Chiral symmetry, strangeness and resonances

M.F.M. LUTZ<sup>a,b</sup>, E.E. KOLOMEITSEV<sup>c</sup> and C.L. KORPA<sup>d</sup>

<sup>a</sup>*Gesellschaft für Schwerionenforschung GSI, Postfach 110552  
D-64220 Darmstadt, Germany*

<sup>b</sup>*Institut für Kernphysik, TU Darmstadt  
D-64289 Darmstadt, Germany*

<sup>c</sup>*The Niels Bohr Institute, Blegdamsvej 17  
DK-2100 Copenhagen, Denmark*

<sup>d</sup>*Department of Theoretical Physics, University of Pecs,  
Ifjusag u. 6, 7624 Pecs, Hungary*

We review the important role played by the chiral SU(3) symmetry in predicting the properties of antikaons and hyperon resonances in cold nuclear matter. Objects of crucial importance are the meson-baryon scattering amplitudes obtained within the chiral coupled-channel effective field theory. The formation of baryon resonances as implied by chiral coupled-channel dynamics is discussed. Results for antikaon and hyperon-resonance spectral functions are presented for isospin symmetric and asymmetric matter.

### §1. Introduction

In this talk we review the application of chiral coupled-channel dynamics to nuclear matter properties of the antikaon, the  $\Lambda(1405)$  s-wave resonance and the  $\Sigma(1385)$  p-wave resonance. A softening of the antikaon mode in nuclear could have been already anticipated in the 70's from K-matrix analysis of the antikaon-nucleon scattering data (see e.g.<sup>1)</sup>) which predicted considerable attraction in the subthreshold s-wave  $K^-$  nucleon scattering amplitudes. In conjunction with the low-density theorem<sup>2),3)</sup> this leads to an antikaon spectral function in nuclear matter that has significant strength at energies smaller than the kaon mass. As was pointed out first in<sup>4)</sup> the realistic evaluation of the antikaon self energy in nuclear matter requires a self consistent scheme. The feedback effect of the antikaon spectral function on the antikaon-nucleon scattering process was found to be important for the hyperon resonance structure in nuclear matter. In turn the modified structure of the hyperon resonances influences the spectral function of the antikaon.

We present and discuss up-to-date results for the spectral functions of antikaons in symmetric and asymmetric cold nuclear matter that are based on a chiral-coupled channel analysis of meson-baryon scattering data.<sup>5)-7)</sup> Unfortunately the empirical data set still leaves much room for different theoretical interpretations, in particular for the subthreshold scattering amplitudes that determine the amount of attraction an antikaon is subject to in cold nuclear matter. Until recently acceptable effective field theories were much less developed in the strangeness sectors as compared to the strangeness zero sector. As a consequence different analysis lead to scattering amplitudes that differ by about a factor two at subthreshold energies ( see<sup>8),9)</sup>).

Thus, it is useful to review also in detail effective coupled-channel field theories based on the chiral Lagrangian.

The task to construct a systematic effective field theory for the meson-baryon scattering processes in the resonance region is closely linked to the fundamental question as to what is the 'nature' of baryon resonances. The radical conjecture<sup>5), 10)–12)</sup> that meson and baryon resonances not belonging to the large- $N_c$  ground states are generated by coupled-channel dynamics lead to a series of works<sup>13)–18)</sup> demonstrating the crucial importance of coupled-channel dynamics for resonance physics in QCD. This conjecture was challenged by a phenomenological model,<sup>11)</sup> which generated successfully non-strange s- and d-wave resonances by coupled-channel dynamics describing a large body of pion and photon scattering data. Of course, the idea to explain resonances in terms of coupled-channel dynamics is an old one going back to the 60's.<sup>19)–24)</sup> For a comprehensive discussion of this issue we refer to.<sup>12)</sup> In recent works,<sup>13), 14)</sup> which will be reviewed here, it was shown that chiral dynamics as implemented by the  $\chi$ -BS(3) approach<sup>5), 10), 12), 25)</sup> provides a parameter-free leading-order prediction for the existence of a wealth of strange and non-strange s- and d-wave wave baryon resonances. A quantitative description of the low-energy pion-, kaon and antikaon scattering data was achieved earlier within the  $\chi$ -BS(3) scheme upon incorporating chiral correction terms.<sup>5)</sup>

## §2. Effective field theory of chiral coupled-channel dynamics

Consider for instance the rich world of antikaon-nucleon scattering illustrated in Fig. 1. The figure clearly illustrates the complexity of the problem. The  $\bar{K}N$  state couples to various inelastic channel like  $\pi\Sigma$  and  $\pi\Lambda$ , but also to baryon resonances below and above its threshold. The goal is to bring order into this world seeking a description of it based on the symmetries of QCD. For instance, as will be detailed below, the  $\Lambda(1405)$  and  $\Lambda(1520)$  resonances will be generated by coupled-channel dynamics, whereas the  $\Sigma(1385)$  should be considered as a 'fundamental' degree of freedom. Like the nucleon and hyperon ground states the  $\Sigma(1385)$  enters as an explicit field in the effective Lagrangian set up to describe the  $\bar{K}N$  system.

The starting point to describe the meson-baryon scattering process is the chiral SU(3) Lagrangian (see e.g.<sup>5), 26)</sup>). A systematic approximation scheme arises due to a successful scale separation justifying the chiral power counting rules.<sup>27)</sup> The effective field theory of the meson-baryon scattering processes is based on the assumption

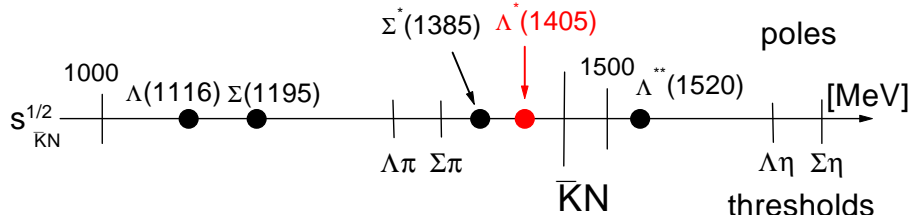


Fig. 1. The world of antikaon-nucleon scattering

that the scattering amplitudes are perturbative at subthreshold energies with the expansion parameter  $Q/\Lambda_\chi$ . The small scale  $Q$  is to be identified with any small momentum of the system. The chiral symmetry breaking scale is

$$\Lambda_\chi \simeq 4\pi f \simeq 1.13 \text{ GeV},$$

with the parameter  $f \simeq 90$  MeV determined by the pion decay process. Once the available energy is sufficiently high to permit elastic two-body scattering a further typical dimensionless parameter  $m_K^2/(8\pi f^2) \sim 1$  arises.<sup>5), 10), 25)</sup> Since this ratio is uniquely linked to two-particle reducible diagrams it is sufficient to sum those diagrams keeping the perturbative expansion of all irreducible diagrams, i.e. the coupled-channel Bethe-Salpeter equation has to be solved. This is the basis of the  $\chi$ -BS(3) approach developed in.<sup>5), 10), 25), 28), 29)</sup>

At leading order in the chiral expansion one encounters the famous Weinberg-Tomozawa<sup>30)</sup> interaction,

$$\begin{aligned} \mathcal{L}_{WT} = & \frac{i}{8f^2} \text{tr} \left( (\bar{B} \gamma^\mu B) \cdot [\Phi, (\partial_\mu \Phi)]_- \right) \\ & + \frac{3i}{8f^2} \text{tr} \left( (\bar{B}_\nu \gamma^\mu B^\nu) \cdot [\Phi, (\partial_\mu \Phi)]_- \right), \end{aligned} \quad (2.1)$$

where we dropped additional structures that do not contribute to the on-shell scattering process at tree level. The terms in (2.1) constitute the leading order s-wave interaction of Goldstone bosons ( $\Phi$ ) with the baryon-octet ( $B$ ) and baryon-decuplet ( $B_\mu$ ) states. The octet and decuplet fields,  $\Phi, B$  and  $B_\mu$ , posses an appropriate matrix structure according to their SU(3) tensor representation.

The scattering process is described by the amplitudes that follow as solutions of the Bethe-Salpeter equation,

$$\begin{aligned} T(\bar{k}, k; w) = & K(\bar{k}, k; w) + \int \frac{d^4 l}{(2\pi)^4} K(\bar{k}, l; w) G(l; w) T(l, k; w), \\ G(l; w) = & -i D(\frac{1}{2}w - l) S(\frac{1}{2}w + l), \end{aligned} \quad (2.2)$$

where we suppress the coupled-channel structure for simplicity. The meson and baryon propagators,  $D(q)$  and  $S(p)$ , are used in the notation of.<sup>11)</sup> We apply the convenient kinematics:

$$w = p + q = \bar{p} + \bar{q}, \quad k = \frac{1}{2}(p - q), \quad \bar{k} = \frac{1}{2}(\bar{p} - \bar{q}), \quad (2.3)$$

where  $q, p, \bar{q}, \bar{p}$  the initial and final meson and baryon 4-momenta. The Bethe-Salpeter scattering equation is recalled for the case of meson baryon-octet scattering. An analogous equation holds for meson baryon-decuplet scattering process (see e.g.<sup>11)</sup>).

The scattering amplitude  $T(\bar{k}, k; w)$  decouples into various sectors characterized by isospin ( $I$ ) and strangeness ( $S$ ) quantum numbers. In the case of meson baryon-octet and baryon-decuplet scattering the following channels are relevant

$$(I, S)_{[8 \otimes 8]} = (0, -3), (1, -3), (\frac{1}{2}, -2), (\frac{3}{2}, -2), (0, -1),$$

$$\begin{aligned}
& (1, -1), (2, -1), \left(\frac{1}{2}, 0\right), \left(\frac{3}{2}, 0\right), (0, 1), (1, 1), \\
& (I, S)_{[8 \otimes 10]} = \left(\frac{1}{2}, -4\right), (0, -3), (1, -3), \left(\frac{1}{2}, -2\right), \left(\frac{3}{2}, -2\right), (0, -1), \\
& \quad (1, -1), (2, -1), \left(\frac{1}{2}, 0\right), \left(\frac{3}{2}, 0\right), \left(\frac{5}{2}, 0\right), (1, 1), (2, 1). \tag{2.4}
\end{aligned}$$

Referring to the detailed discussion given in<sup>5),15)</sup> we assume a systematic on-shell reduction of the Bethe-Salpeter interaction kernel. We introduce an on-shell equivalent effective interaction kernel  $V$ , together with three off-shell interaction kernels  $V_L$ ,  $V_R$  and  $V_{LR}$  where  $V_R$  ( $V_L$ ) vanishes if the initial (final) particles are on-shell. The interaction kernel  $V_{LR}$  is defined to vanish if evaluated with either initial or final particles on-shell. The latter objects are defined by:

$$\begin{aligned}
K = & V + (1 - V \cdot G) \cdot V_L + V_R \cdot (1 - G \cdot V) \\
& + (1 - V \cdot G) \cdot V_{LR} \cdot (1 - G \cdot V) - V_R \cdot \frac{1}{1 - G \cdot V_{LR}} \cdot G \cdot V_L. \tag{2.5}
\end{aligned}$$

The decomposition of the Bethe-Salpeter interaction kernel is unique and can be applied to an arbitrary interaction kernel once it is defined what is meant with the 'on-shell' part of any two-particle amplitude. The latter we define as the part of the amplitude that has a decomposition into the complete set of projectors

$$V(\bar{k}, k; w) = \sum_{J, P, a, b} V_{ab}^{(JP)}(\sqrt{s}) \mathcal{Y}_{ab}^{(JP)}(\bar{q}, q; w), \tag{2.6}$$

where the projectors carry good total angular momentum  $J$  and parity  $P$ . The merit of the projectors is that they decouple the Bethe-Salpeter equation (2.2) into orthogonal sectors labeled by the total angular momentum,  $J$ , and parity,  $P$ . We emphasize that the projectors have also the important property that they are applicable in the case of intermediate states that have broad spectral distributions. It is clear that performing a chiral expansion of  $K$  and  $V$  to some order  $Q^n$  leads to a straight forward identification of the off-shell kernels  $V_L$ ,  $V_R$  and  $V_{LR}$  to the same accuracy.

The on-shell part of the scattering amplitude takes the simple form,

$$\begin{aligned}
T^{\text{on-shell}}(\bar{k}, k; w) &= \sum_{J, P} M^{(JP)}(\sqrt{s}) \mathcal{Y}^{(JP)}(\bar{q}, q; w), \\
M^{(JP)}(\sqrt{s}) &= \left[ 1 - V^{(JP)}(\sqrt{s}) J^{(JP)}(\sqrt{s}) \right]^{-1} V^{(JP)}(\sqrt{s}), \tag{2.7}
\end{aligned}$$

with a set of divergent loop functions  $J^{(JP)}(\sqrt{s})$ . We insist on the renormalization condition,

$$T^{(I, S)}(\bar{k}, k; w) \Big|_{\sqrt{s}=\mu(I, S)} = V^{(I, S)}(\bar{k}, k; w) \Big|_{\sqrt{s}=\mu(I, S)}, \tag{2.8}$$

together with the natural choice for the subtraction points,

$$\begin{aligned}
\mu(I, +1) &= \mu(I, -3) = \frac{1}{2}(m_A + m_\Sigma), \quad \mu(I, 0) = m_N, \\
\mu(0, -1) &= m_A, \quad \mu(1, -1) = m_\Sigma, \quad \mu(I, -2) = \mu(I, -4) = m_\Xi, \tag{2.9}
\end{aligned}$$

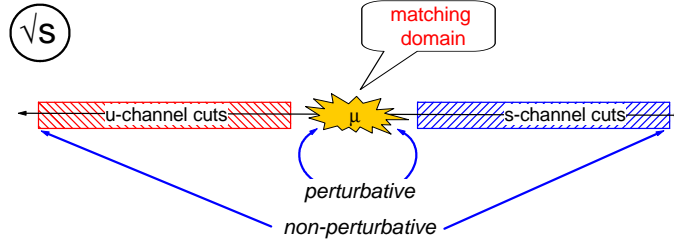


Fig. 2. Graphical illustration for the gluing of s- and u-channel unitarized scattering amplitudes

as explained in detail in.<sup>5),13),14)</sup> The renormalization condition reflects the basic assumption our effective field theory is based on, namely that at subthreshold energies the scattering amplitudes can be evaluated in standard chiral perturbation theory. This is achieved by supplementing (2.2) with (2.8,2.9). The subtraction points (2.9) are the unique choices that protect the s-channel baryon-octet masses manifestly in the p-wave  $J = \frac{1}{2}$  scattering amplitudes.

It is useful to elaborate in some detail on the structure of the loop functions. The merit of the projector technique is that dimensional regularization can be used to evaluate the latter ones. Here we exploit the result that any given projector is a finite polynomial in the available 4-momenta. This implies that the loop functions can be expressed in terms of a log-divergent master function,  $I(\sqrt{s})$ , and reduced tadpole terms,

$$J^{(JP)}(\sqrt{s}) = N^{(JP)}(\sqrt{s}) \left[ I(\sqrt{s}) - I(\mu) \right],$$

$$I(\sqrt{s}) = \frac{1}{16\pi^2} \left( \frac{p_{cm}}{\sqrt{s}} \left( \ln \left( 1 - \frac{s - 2p_{cm}\sqrt{s}}{m^2 + M^2} \right) - \ln \left( 1 - \frac{s + 2p_{cm}\sqrt{s}}{m^2 + M^2} \right) \right) \right. \\ \left. + \left( \frac{1}{2} \frac{m^2 + M^2}{m^2 - M^2} - \frac{m^2 - M^2}{2s} \right) \ln \left( \frac{m^2}{M^2} \right) + 1 \right) + I(0), \quad (2.10)$$

where  $\sqrt{s} = \sqrt{M^2 + p_{cm}^2} + \sqrt{m^2 + p_{cm}^2}$ . The normalization factor  $N_a^{(JP)}(\sqrt{s})$  is a polynomial in  $\sqrt{s}$  and the mass parameters. In (2.10) the renormalization scale dependence of the scalar loop function  $I(\sqrt{s})$  was traded in favor of a dependence on a subtraction point  $\mu$ , leading to compliance with the renormalization condition (2.8). The loop functions  $J^{(J,P)}(\sqrt{s})$  are consistent with chiral counting rules only if the subtraction scale  $\mu \simeq M$  is chosen close to the 'heavy' hadron mass.<sup>5),25)</sup> Moreover it was shown that keeping reduced tadpole terms in the loop functions leads to a renormalization of s-channel exchange terms that is in conflict with chiral counting rules if the effective interaction kernel is evaluated in perturbation theory.<sup>5)</sup>

The merit of the scheme<sup>5),10),25)</sup> lies in the property that for instance the  $K \Xi$  and  $\bar{K} \Xi$  scattering amplitudes match at  $\sqrt{s} \sim m_\Xi$  approximately as expected from crossing symmetry. In<sup>5),15)</sup> we suggested to glue s- and u-channel unitarized scattering amplitudes at subthreshold energies as illustrated in Fig. 3. This reflects the basic assumption that diagrams showing an s-channel or u-channel unitarity cut need to be summed to all orders at least at energies close to where the diagrams

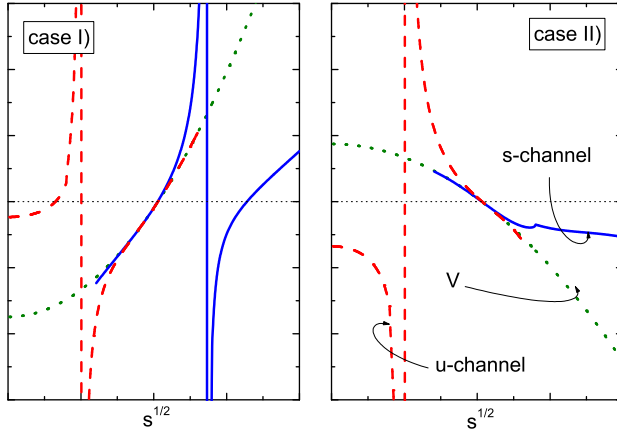


Fig. 3. Illustration of the gluing of s- and u-channel unitarized scattering amplitudes for two typical cases. The lines extending to the right (left) are the results of a s-channel (u-channel) unitarization. The dotted lines represent the contribution of the effective interaction kernel  $V$

develop their imaginary part. By construction, a glued scattering amplitude satisfies crossing symmetry exactly at energies where the scattering process takes place. At subthreshold energies crossing symmetry is implemented approximatively only, however, to higher and higher accuracy when more chiral correction terms are considered. Insisting on the renormalization condition (2.8,2.9) guarantees that subthreshold amplitudes match smoothly and therefore the final 'glued' amplitudes comply with the crossing-symmetry constraint to high accuracy. Fig. 3 illustrates this mechanism for two typical cases.<sup>15)</sup> Whereas in case I) both the s- and u-channel unitarizations lead to bound states, in case II) only the u-channel unitarization generates a bound state. For simplicity the figure does not show the additional complications present in the meson-baryon forward scattering amplitude, that are due to pole structures implied by the baryon octet ground states.<sup>5)</sup> It is amusing to observe that the natural subtraction points (2.9) can also be derived if one incorporates photon-baryon inelastic channels. Then additional constraints arise. For instance the reaction  $\gamma \Xi \rightarrow \gamma \Xi$ , which is subject to a crossing symmetry constraint at threshold, may go via the intermediate states  $\bar{K} \Lambda$  or  $\bar{K} \Sigma$ .

The perturbative nature of subthreshold amplitudes, a crucial assumption of the  $\chi$ -BS(3) approach proposed in,<sup>5),10),25)</sup> is not necessarily true in phenomenological coupled-channel schemes in.<sup>31)–36)</sup> Using the subtraction scales as free parameters, as advocated in,<sup>34)–36)</sup> may be viewed as promoting the counter terms of chiral order  $Q^3$  to be unnaturally large. If the subtraction scales are chosen far away from their natural values (2.9) the resulting loop functions are in conflict with chiral power counting rules.<sup>25)</sup> Though unnaturally large  $Q^3$  counter terms can not be excluded from first principals one should check such an assumption by studying corrections terms systematically. A detailed test of the naturalness of the  $Q^3$  counter terms was performed within the  $\chi$ -BS(3) scheme<sup>5)</sup> demonstrating good convergence in the channels studied without any need for promoting the counter terms of order

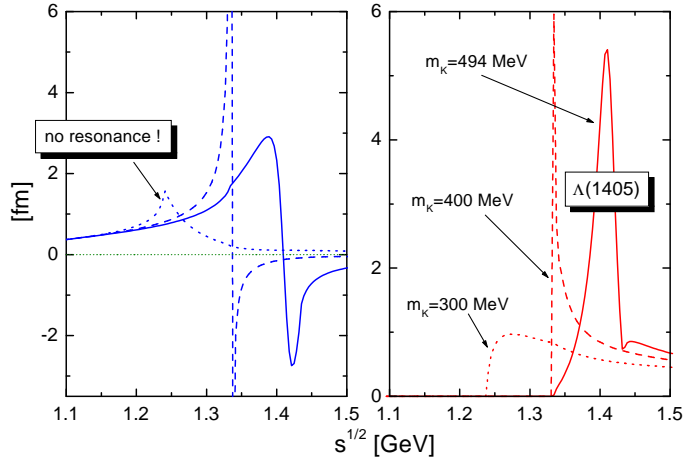


Fig. 4. S-wave antikaon-nucleon scattering amplitude in the isospin zero channel as it follows in the  $\chi$ -BS(3) approach at leading order.

$Q^3$ . Possible correction terms in the approach followed in<sup>34)–36)</sup> have so far not been studied systematically for meson-baryon scattering. Moreover, if the scheme advocated in<sup>34)–36)</sup> were applied in all eleven isospin strangeness sectors with  $J^P = \frac{1}{2}^-$  a total number of 26 subtraction parameters arise. This should be compared with the only ten counter terms of chiral order  $Q^3$  contributing to the on-shell scattering amplitude at that order.<sup>5)</sup> Selecting only the operators that are leading in the large- $N_c$  limit of QCD out of the ten  $Q^3$  operators only four survive.<sup>5)</sup> We conclude that it would be inconsistent to apply the approach used in<sup>34)–36)</sup> in all isospin strangeness channels without addressing the above mismatch of parameters. Our scheme has the advantage over the one in<sup>34)–36)</sup> that once the parameters describing subleading effects are determined in a subset of sectors one has immediate predictions for all sectors ( $I, S$ ). A mismatch of the number of parameters is avoided altogether since the  $Q^3$  counter terms enter the effective interaction kernel directly.

Given the subtraction scales (2.9) the leading order calculation is parameter free. Of course chiral correction terms do lead to further so far unknown parameters which need to be adjusted to data. Within the  $\chi$ -BS(3) approach such correction terms enter the effective interaction kernel  $V$  rather than leading to subtraction scales different from (2.9) as it is assumed in<sup>34)–36)</sup>. In particular the leading correction effects are determined by the counter terms of chiral order  $Q^2$ .

The  $\chi$ -BS(3) scheme was applied first in<sup>10),25)</sup> where results for the antikaon-nucleon scattering amplitudes at leading and subleading orders were presented. In particular it was demonstrated that the  $\Lambda(1405)$  resonance is generated by coupled-channel dynamics without the need of adjusting any parameter.<sup>25)</sup> This is an important result because it avoided for the first time the use of a fine-tuned cutoff parameter which is at odds with chiral counting rules. The isospin zero s-wave scattering amplitude as it followed at leading order is shown in Fig. 3, which clearly illustrates the presence of the  $\Lambda(1405)$  resonance. Lowering the strange current quark mass of QCD has a dramatic effect on the resonance structure. Chiral-coupled chan-

nel dynamics predicts that in a world with kaons of mass 300 MeV the  $\Lambda(1405)$  resonance would not exist. This is a clear prediction that can be tested with Lattice QCD simulations.<sup>38)–41)</sup> Moreover the figure reflects the matching of the unitarized scattering amplitude with the effective interaction kernel at subthreshold energies. As a consequence of the defining assumption of the  $\chi$ -BS(3) approach, namely, that the subthreshold scattering amplitudes remain perturbative, all lines in the figure representing the real part of the scattering amplitude join at subthreshold energies. This follows since the effective interaction kernel does not depend on the kaon mass at leading order.<sup>5)</sup>

### §3. Baryon resonances from chiral SU(3) symmetry

There is a long standing controversy to what is the nature of s-wave baryon resonances. Before the event of the quark model several such states have been successfully generated in terms of coupled-channels dynamics.<sup>19)–23)</sup> A prime example is the  $\Lambda(1405)$  resonance, discussed already in the previous section, and which was successfully described already in the latter works. These early calculations are closely related to modern approaches based on the leading-order chiral SU(3) Lagrangian. The interaction used in<sup>19)–23)</sup> matches the Weinberg-Tomozawa interaction (2.1) if expanded in a Taylor series.<sup>24)</sup> The main difference of the early attempts from computations based on the chiral Lagrangian is the way the coupled-channel scattering equation is regularized and renormalized. The crucial advance over the last years in this field is therefore a significant improvement of the systematics, i.e. how to implement corrections terms into coupled-channel dynamics.

We give a discussion of the s- and d-wave baryon resonance spectrum that arises in chiral-coupled effective field theory based on the leading order chiral Lagrangian.<sup>13),14)</sup> Consider first the the SU(3) limit. The latter is not defined uniquely depending on the magnitude of the current quark masses,  $m_u = m_d = m_s$ . We study two scenarios.<sup>13),14)</sup> In the 'light' SU(3) limit the current quark masses are chosen such that one obtains  $m_\pi = m_K = m_\eta = 140$  MeV. The second case, the 'heavy' SU(3) limit, is characterized by  $m_\pi = m_K = m_\eta = 500$  MeV.

The  $J^P = \frac{1}{2}^-$  baryon resonances manifest themselves as poles in the s-wave meson baryon-octet scattering amplitudes. In the SU(3) limit the latter decompose according to,

$$8 \otimes 8 = 27 \oplus \overline{10} \oplus 10 \oplus 8 \oplus 8 \oplus 1 \quad (3.1)$$

The leading order chiral Lagrangian (2.1) predicts attraction in the two octet and the singlet channel but repulsion in the 27-plet and decuplet channels. In the 'heavy' SU(3) limit the chiral dynamics predicts two degenerate octet bound states together with a non-degenerate singlet state.<sup>13),13),14),19)–23),36)</sup> However, in the 'light' SU(3) limit all states disappear leaving no clear resonance signal.

In the  $J^P = \frac{3}{2}^-$  sector the resonances properties are studied in terms of the s-wave meson baryon-decuplet scattering amplitudes. In this case the Weinberg-Tomozawa interaction (2.1) is attractive in the octet, decuplet and 27-plet channel,

but repulsive in the 35-plet channel,

$$8 \otimes 10 = 35 \oplus 27 \oplus 10 \oplus 8. \quad (3.2)$$

Therefore one may expect resonances or bound states in the former channels. Indeed, in the 'heavy' SU(3) limit  $72 = 4 \times (8+10)$  bound states are generated in this sector forming an octet and decuplet representation of the SU(3) group. A 27-plet-bound state is not observed. This reflects the weaker attraction in that channel. However, if one artificially increases the amount of attraction by about 40 % by lowering the value of  $f$  in the Weinberg-Tomozawa term, a clear bound state arises in this channel also. A contrasted result is obtained if one lowers the meson masses down to the pion mass arriving at the 'light' SU(3) limit. Then we find neither bound nor resonance octet or decuplet states. This pattern is a clear prediction of chiral couple-channel dynamics which should be tested with unquenched QCD lattice simulations.<sup>38)-41)</sup>

Using physical meson and baryon masses the bound-state turn into resonances as shown in Figs. 5,6 in terms of speed plots. In<sup>14)</sup> we generalized the notion of a speed<sup>42)</sup> to the case of coupled-channels in a way that the latter reveals the coupling strength of a given resonance to any channel, closed or open. The merit of producing speed plot lies in a convenient property of the latter allowing a straight forward extraction of resonance parameters. Assume that a coupled-channel amplitude  $M_{ab}(\sqrt{s})$  develops a pole of mass  $m_R$ , with

$$M_{ab}(\sqrt{s}) = -\frac{g_a^* g_b m_R}{\sqrt{s} - m_R + i \Gamma/2}, \quad \Gamma_a = \frac{|g_a|^2}{4\pi} |p_{cm}^{(a)}| N_a(m_R), \quad (3.3)$$

where the total resonance width,  $\Gamma$ , is given by the sum of all partial widths. The normalization factor  $N(m_R)$  in (3.3) is identical to the one entering the form of the loop functions in (2.10). The speed plots take a maximum at the resonance mass  $\sqrt{s} = m_R$ , with

$$\text{Speed}_{aa}(m_R) = \begin{cases} 2 \frac{\Gamma_a}{\Gamma^2} \left| 2 \sum_c \frac{\Gamma_c}{\Gamma} - 1 \right| & \text{if } a = \text{open} \\ 2 \frac{\Gamma_a}{\Gamma^2} \left| 2 \sum_c \frac{\Gamma_c}{\Gamma} - i \right| & \text{if } a = \text{closed}, \end{cases} \quad (3.4)$$

$$\Gamma = \sum_{a=\text{open}} \Gamma_a.$$

The result (3.4) clearly demonstrates that the speed of a resonance in a given open channel  $a$  is not only a function of the total width parameter  $\Gamma$  and the partial width  $\Gamma_a$ . It does depend also on how strongly closed channels couple to that resonance. This is in contrast to the delay time of a resonance for which closed channels do not contribute. In the case of s-wave resonances thresholds induce square-root singularities which should not be confused with a resonance signal.

The speed plots of Fig. 5 show evidence for the formation of the  $\Xi(1690)$ ,  $\Lambda(1405)$ ,  $\Lambda(1670)$  and  $N(1535)$  resonances close to their empirical masses. An additional  $(I, S) = (0, -1)$  state, which couples strongly to the  $\pi\Sigma$  channel,<sup>13),36)</sup> can be found as a complex pole in the scattering amplitude close to the pole implied by the  $\Lambda(1405)$  resonance. There is no clear signal for  $(I, S) = (1, -1)$  resonances at

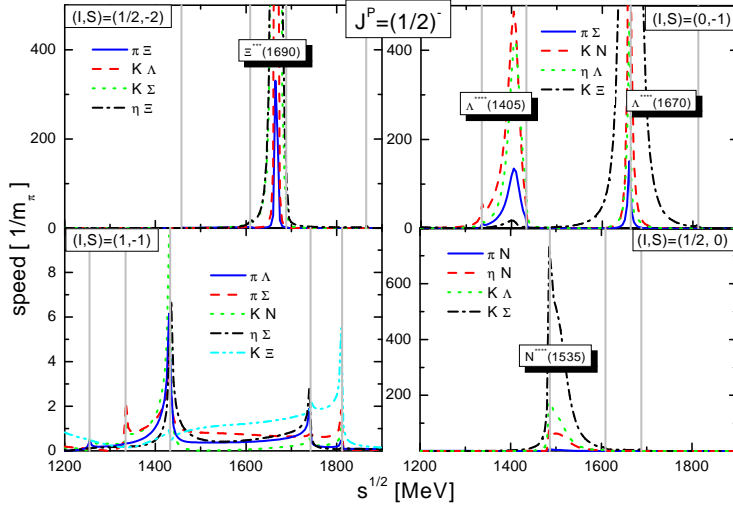


Fig. 5. Diagonal speed plots of the  $J^P = \frac{1}{2}^-$  sector. The vertical lines show the opening of inelastic meson baryon-decuplet channels. Parameter-free results are obtained in terms of physical masses and  $f = 90$  MeV.<sup>13), 14)</sup>

this leading order calculation. However, chiral corrections lead to a clear signal in this sector<sup>5)</sup> suggesting a state that may be identified with the  $\Sigma(1750)$  resonance, the only well established s-wave resonance in this sector. The fact that a second resonance with  $(I, S) = (\frac{1}{2}, 0)$  is not seen in Fig. 5, even though the 'heavy' SU(3) limit suggests its existence, may be taken as a confirmation of the phenomenological observation<sup>11)</sup> that the  $N(1650)$  resonance couples strongly to the  $\omega_\mu N$  channel not considered here.

In Fig. 6 speed plots of the  $J^P = \frac{3}{2}^-$  sector are shown for all channels in which octet and decuplet resonance states are expected. It is a remarkable success of the  $\chi$ -BS(3) approach that it predicts the four star hyperon resonances  $\Xi(1820)$ ,  $\Lambda(1520)$ ,  $\Sigma(1670)$  with masses quite close to the empirical values. The nucleon and isobar resonances  $N(1520)$  and  $\Delta(1700)$  also present in Fig. 6, are predicted with less accuracy. The important result here is the fact that those resonances are generated at all. It should not be expected to obtain already fully realistic results in this leading order calculation. For instance chiral correction terms are expected to provide a d-wave  $\pi \Delta$ -component of the  $N(1520)$ . We continue with the peak in the (0,3)-speeds at mass 1950 MeV. Since this is below all thresholds it is in fact a bound state. Such a state has so far not been observed but is associated with a decuplet resonance.<sup>37)</sup> Further states belonging to the decuplet are seen in the  $(\frac{1}{2}, -2)$ - and  $(1, -1)$ -speeds at masses 2100 MeV and 1920 MeV. The latter state can be identified with the three star  $\Xi(1940)$  resonance. Finally we point at the fact that the (0, -1)-speeds show signals of two resonance states consistent with the existence of the four star resonance  $\Lambda(1520)$  and  $\Lambda(1690)$  even though in the 'heavy' SU(3) limit we observed only one bound state. It appears that the SU(3) symmetry breaking pattern generates the 'missing' state in this particular sector by promoting

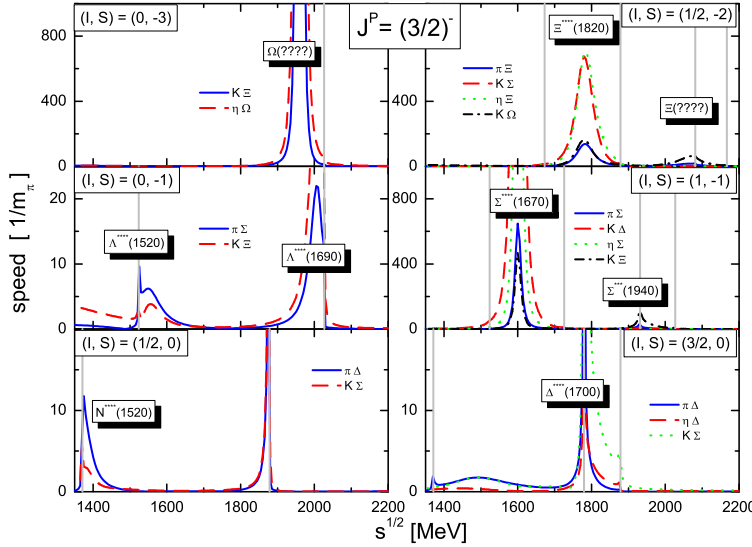


Fig. 6. Diagonal speed plots of the  $J^P = \frac{3}{2}^-$  sector. The vertical lines show the opening of inelastic meson baryon-decuplet channels. Parameter-free results are obtained in terms of physical masses and  $f = 90$  MeV.

the weak attraction of the 27-plet contribution in (3.2).

#### §4. Chiral correction terms and scattering data

The present data set for antikaon-nucleon scattering leaves much room for different theoretical extrapolations to subthreshold energies.<sup>1), 43)-51)</sup> As a consequence the subthreshold  $\bar{K}N$  scattering amplitudes of different analyses may differ by as much as a factor of two<sup>50), 51)</sup> in the region of the  $\Lambda(1405)$  resonance. Thus it is of crucial importance to apply effective field theory methods in order to control the uncertainties. In particular constraints from crossing symmetry and chiral symmetry should be taken into account.

Since the accuracy of the data improves dramatically as the energy increases it is desirable to incorporate contributions from higher partial waves into the analysis. Important information on the p-wave dynamics is provided by angular distributions for the inelastic  $K^-p$  reactions. The available data are represented in terms of coefficients  $A_n$  characterizing the differential cross section  $d\sigma(\cos \theta, \sqrt{s})$  as functions of the center of mass scattering angle  $\theta$  and the total energy  $\sqrt{s}$ :

$$\frac{d\sigma(\sqrt{s}, \cos \theta)}{d \cos \theta} = \sum_{n=0}^{\infty} A_n(\sqrt{s}) P_n(\cos \theta). \quad (4.1)$$

In Fig. 7 we compare the empirical ratios  $A_1/A_0$  and  $A_2/A_0$  with the results of the  $\chi$ -BS(3) approach carried out to chiral order  $Q^3$ .<sup>5)</sup> A large  $A_1/A_0$  ratio is found only in the  $K^-p \rightarrow \pi^0\Lambda$  channel demonstrating the importance of p-wave effects in the isospin one channel. Note the sizeable p-wave contributions at somewhat

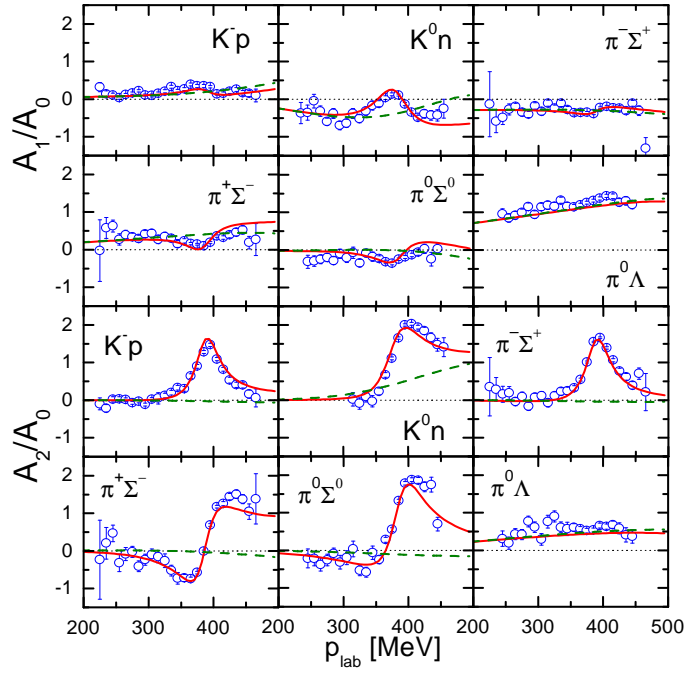


Fig. 7. Coefficients  $A_1$  and  $A_2$  for the  $K^- p \rightarrow \pi^0 \Lambda$ ,  $K^- p \rightarrow \pi^\mp \Sigma^\pm$  and  $K^- p \rightarrow \pi^0 \Sigma$  differential cross sections.<sup>52), 53)</sup> The solid lines are the result of the  $\chi$ -BS(3) approach with inclusion of the d-wave resonances. The dashed lines show the effect of switching off d-wave contributions.

larger momenta seen in the charge-exchange reaction of Fig. 7. The dashed lines of Fig. 7, which are obtained when switching off d-wave contributions, illustrate the importance of the  $\Lambda(1520)$  resonance for the angular distributions in the isospin zero channel. In<sup>5)</sup> the d-wave resonances were not yet generated dynamically rather were introduced as elementary fields. To improve on this it would be necessary to extend the analysis<sup>5)</sup> by incorporating further inelastic channels, like the meson baryon-decuplet channels. Also it would be useful to incorporate the loop-correction effects which give contributions to the effective interaction kernel at chiral order  $Q^3$ . The latter were not yet considered in<sup>5)</sup> based on the expectation that they should be suppressed in the large- $N_c$  limit. The importance of the results<sup>5)</sup> lies in the achievement that for the first time a simultaneous and quantitative description of the low-energy pion-, kaon- and antikaon-nucleon scattering data based on chiral coupled-channel dynamics was obtained. Moreover that analysis demonstrated that all considered counter terms determined by the scattering data have natural size. Though SU(3) symmetry breaking effects are important to achieve a quantitative description of the data set they are small and justify the application of the chiral SU(3) Lagrangian.

### §5. Self consistent strangeness propagation in cold nuclear matter

Once the microscopic interaction of the Goldstone bosons with the constituents of nuclear matter is understood one may study the properties of Goldstone bosons in nuclear matter. Not only from an experimental but also from a theoretical point of view the pions and kaons, the lightest excitation of the QCD vacuum with masses of 140 MeV and 495 MeV respectively, are outstanding probes for exciting many-body dynamics. The Goldstone bosons are of particular interest since their in-medium properties reflect the structure of the nuclear many-body ground state. For example at high baryon densities one expects the chiral symmetry to be restored. One therefore anticipates that the Goldstone bosons change their properties substantially as one compresses nuclear matter. A possible consequence of a significantly reduced effective  $K^-$  mass suggested first by Kaplan and Nelson<sup>54)</sup> could be that kaons condense in the interior of neutron stars.<sup>55)–58)</sup> A complementary suggestion was recently put forward by Yamazaki and Akaishi<sup>59)</sup> that the attractive antikaon-proton force is sufficiently strong to form high-density few-particle clusters. In this review we do not touch neither of the two exciting topics. To address properties of antikaons at high-density or localized strangeness systems is beyond our present scope. Our goal is to derive the properties of antikaons in nuclear matter densities not too large, say up to twice nuclear matter saturation density, from the microscopic interaction of antikaons with the nucleons. This is relevant for the description of kaonic atom data as well as for the understanding of subthreshold antikaon production in heavy ion collisions as studied in detail at GSI.<sup>60)</sup>

Even though in the SU(3) limit of QCD with degenerate current quark masses  $m_u = m_d = m_s$  the pions and kaons have identical properties with respect to the strong interactions, they provide very different means to explore the nuclear many-body system. This is because the SU(3) symmetry is explicitly broken by a nuclear matter state with strangeness density zero, a typical property of matter produced in the laboratory. A pion, if inserted into isospin degenerate nuclear matter, probes rather directly the spontaneously broken or possibly restored chiral SU(2) symmetry. A kaon, propagating in strangeness free nuclear matter, loses its Goldstone boson character since the matter by itself explicitly breaks the SU(3) symmetry. It is subject to three different phenomena: the spontaneously broken chiral SU(3) symmetry, the explicit symmetry breaking of the small current quark masses and the explicit symmetry breaking of the nuclear matter bulk. The various effects are illustrated by recalling the effective pion and kaon masses in a dilute isospin symmetric nuclear matter gas. The low-density theorem<sup>2),3)</sup> predicts mass changes  $\Delta m_\Phi^2$  for any meson  $\Phi$  in terms of its isospin averaged s-wave meson-nucleon scattering length  $a_{\Phi N}$

$$\Delta m_\Phi^2 = -4\pi \left(1 + \frac{m_\Phi}{m_N}\right) a_{\Phi N} \rho + \mathcal{O}(\rho^{4/3}) \quad (5.1)$$

where  $\rho$  denotes the nuclear density. According to the above arguments one expects that the pion-nucleon scattering length  $a_{\pi N} \propto m_\pi^2$  must vanish in the chiral SU(2) limit since isospin symmetric nuclear matter conserves the Goldstone boson character of the pions at least at small densities. On the other hand, kaons loose

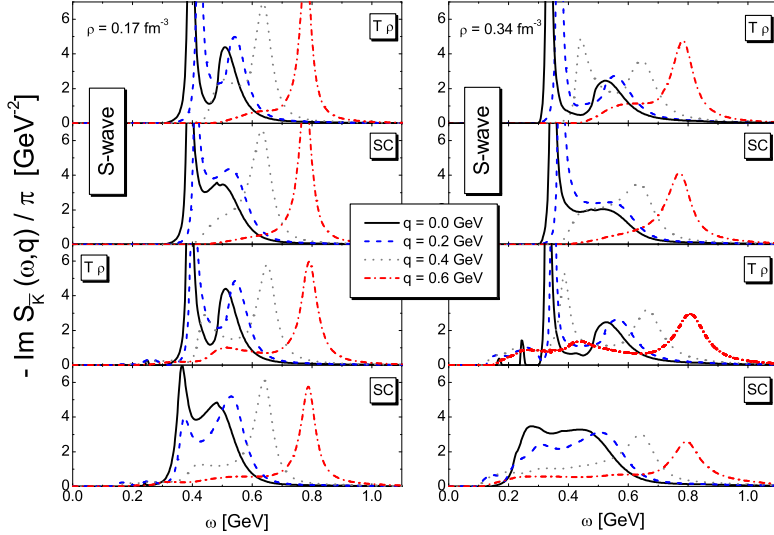


Fig. 8. Antikaon spectral function as a function of antikaon energy  $\omega$  and momentum  $\vec{q}$ . The labels 'T $\rho$ ' and 'SC' refer to calculations obtained in terms of free-space and in-medium  $\bar{K}N$  amplitudes respectively. The first two rows give the results with only s-wave interactions and the last two rows with all s-, p- and d-wave contributions.

their Goldstone boson properties in strangeness-free matter and therefore one expects  $a_{K\bar{N}} \propto m_K$  and in particular  $a_{K^-N} \neq a_{K^+N}$ . This is demonstrated by the Weinberg-Tomozawa theorem (see (2.1)) which predicts the s-wave scattering length in terms of the chiral order parameter  $f \simeq 90$  MeV :

$$a_{\pi N} = 0 + \mathcal{O}(m_\pi^2), \quad a_{K^\pm N} = \mp \frac{m_K}{4\pi f^2} + \mathcal{O}(m_K^2). \quad (5.2)$$

In the pion sector the Weinberg-Tomozawa theorem (5.2) is beautifully confirmed by the smallness of the empirical isospin averaged pion-nucleon scattering length  $a_{\pi N} \simeq -0.01$  fm. In the kaon sector the Weinberg-Tomozawa theorem misses the empirical scattering  $K^+$  nucleon scattering length  $a_{K^+N} \simeq -0.3$  fm by about a factor of three. Even more spectacular is the disagreement of the Weinberg-Tomozawa term in the  $K^-$  case where (5.2) predicts  $a_{K^-N} \simeq +0.9$  fm while the empirical  $K^-$  nucleon scattering length is about  $a_{K^-N} \simeq (-0.6 + i 1.1)$  fm. Whereas in conjunction with the low-density theorem the Weinberg-Tomozawa theorem predicts a decreased effective  $K^-$  mass, the empirical scattering length unambiguously states that there must be repulsion in the  $K^-$  channel at least at very small nuclear densities.

In nuclear matter there exist multiple modes with quantum numbers of the  $K^-$  resulting from the coupling of the various hyperon states to a nucleon-hole state.<sup>61)</sup> As a consequence the  $K^-$  spectral function shows a rather complex structure as a function of baryon density, kaon energy and momentum. This is illustrated by recalling the low-density theorem as applied for the energy dependence of the kaon

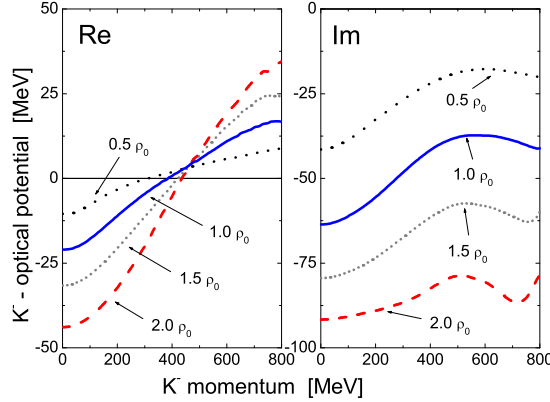


Fig. 9. Antikaon optical potential  $V_{\text{opt.}}(\vec{q}; \rho)$  for isospin symmetric nuclear matter densities. Results are shown for  $0.5 \rho_0$ ,  $1.0 \rho_0$ ,  $1.5 \rho_0$  and  $2.0 \rho_0$  where  $\rho_0 = 0.17 \text{ fm}^{-3}$ .

self energy  $\Pi_{\bar{K}}(\omega, \rho)$ . At zero antikaon momentum the latter,

$$\Pi_{\bar{K}}(\omega, \rho) = -4\pi \left(1 + \frac{\omega}{m_N}\right) f_{\bar{K}N}^{\text{s-wave}}(m_N + \omega) \rho + \mathcal{O}(\rho^{4/3}), \quad (5.3)$$

is determined by the s-wave kaon-nucleon scattering amplitude  $f_{\bar{K}N}^{\text{s-wave}}(\sqrt{s})$  (see e.g.<sup>3)</sup>). A pole contribution to  $\Pi_{\bar{K}}(\omega, \rho)$  from a hyperon state with mass  $m_H$ , if sufficiently strong, may lead to a  $K^-$  like state of approximate energy  $m_H - m_N$ . Most important are the  $\Lambda(1405)$  s-wave resonance and the  $\Sigma(1385)$  p-wave resonance. The realistic evaluation of the antikaon self energy in nuclear matter requires a self-consistent scheme.<sup>4)</sup> In particular the feedback effect of an attractive antikaon spectral function on the antikaon-nucleon scattering process was found to be important for the  $\Lambda(1405)$  resonance structure in nuclear matter. This effect is easily understood from the strong dependence of the antikaon-nucleon scattering amplitude on the kaon mass as demonstrated in Fig. 3. It has striking consequences for the properties of the  $\Lambda(1405)$  resonance in nuclear matter. Contrary to naive expectations<sup>62)</sup> that the effective resonance mass is pushed up to larger values due to the Pauli blocking effect, an attractive mass shift results as a consequence of self consistency.<sup>4), 6)</sup> Ramos and Oset<sup>63)</sup> confirmed this result qualitatively by a calculation applying their phenomenological model.<sup>51)</sup> The quantitative comparison of the original calculation,<sup>4)</sup> which was based on the model of the Munich group,<sup>50)</sup> is hampered by the facts that first the subthreshold amplitudes of<sup>5), 50)</sup> and<sup>51)</sup> differ significantly and second the computation in<sup>63)</sup> relies on an additional approximation that amounts to neglecting the strong momentum dependence of the antikaon self energy (see<sup>9), 12)</sup>). We refrain here from a comparison with the results of Tolos et al.<sup>64)</sup> Their many-body computation includes higher partial-wave contributions but self consistency was implemented relying on a quasi-particle approximation. Moreover, the applied meson-exchange model<sup>48)</sup> was confronted so far with total cross sections data only. Thus, it remains unclear whether it describes the dynamics of

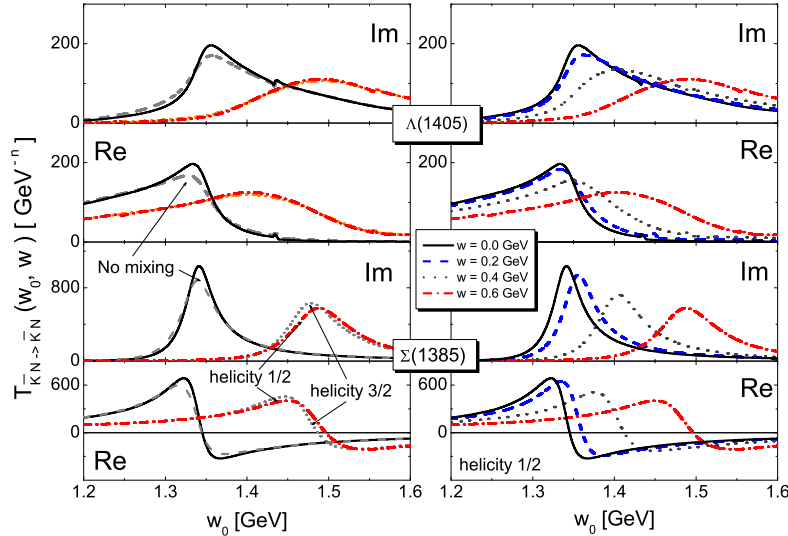


Fig. 10. Hyperon resonance spectral functions for the  $\Lambda(1405)$  and  $\Sigma(1385)$  as a function of the hyperon energy  $w_0$  and momentum  $\vec{w}$  for isospin symmetric nuclear matter. It is shown the s-wave  $I=0$  and p-wave  $I=1$  partial wave amplitudes at  $\rho_n + \rho_p = 0.17 \text{ fm}^{-3}$ . The left hand panels demonstrate the small effect of switching off the mixing of the partial wave amplitudes (dashed versus full lines) and the splitting of the 4 spin  $3/2$  states into helicity one half and three half modes (dotted versus dashed-dotted lines).

higher partial waves correctly. A precise understanding of all these issues is required for a microscopic description of kaonic atoms.<sup>8),9)</sup>

In Fig. 8 the antikaon spectral function evaluated at symmetric nuclear densities  $\rho_0$  and  $2\rho_0$  according to various approximation strategies is shown.<sup>6)</sup> The results are based on antikaon-nucleon scattering amplitudes obtained within the chiral coupled-channel effective field theory,<sup>5)</sup> where s-, p- and d-wave contributions were considered. The many-body computation<sup>6)</sup> was performed in a self consistent manner respecting covariance manifestly. In the first and third rows the antikaon self energy is computed in terms of the free-space scattering amplitudes only. Here the first row gives the result with only s-wave contributions and the third row includes all s-, p- and d-wave contributions. The second and fourth rows give results obtained in the self consistent approach where the full result of the last row includes all partial waves and the results in the second row follow with s-wave contributions only. In all cases a self consistent evaluation of the spectral function leads to dramatic changes in the spectral function as compared to a calculation which is based on the free-space scattering amplitudes only. Moreover, as emphasized in the discussion of the  $\Lambda(1405)$  resonance properties, the effects of higher partial waves are not negligible. This was anticipated first in.<sup>8),25)</sup> As is evident upon comparing the first and third rows of Fig. 8 the p- and d-wave contributions add quite significant attraction for small energies and large momenta. At twice nuclear saturation density most striking is the considerable support of the spectral function at small energies. That reflects in part

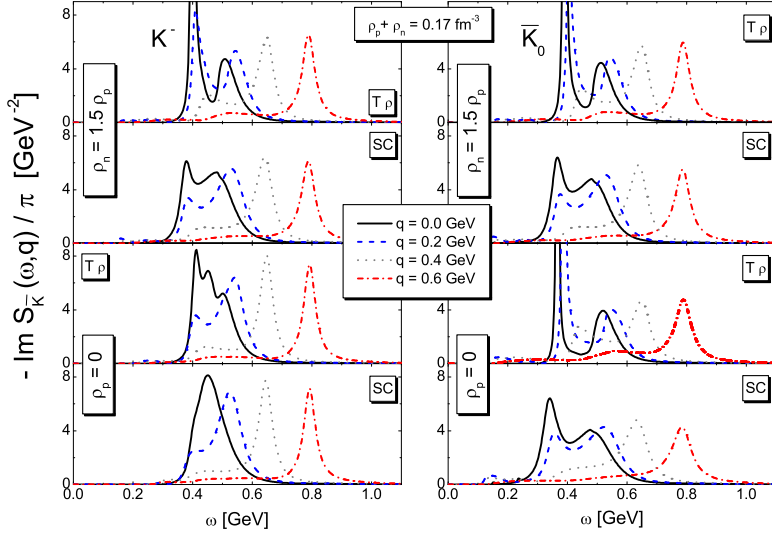


Fig. 11. Antikaon spectral functions as a function of antikaon energy  $\omega$  and momentum  $q$  in asymmetric nuclear matter with  $\rho_p + \rho_n = 0.17 \text{ fm}^{-3}$ . The labels 'T $\rho$ ' and 'SC' refer to calculations obtained in terms of free-space and self consistent in-medium  $\bar{K}N$  amplitudes respectively. The first column gives the result for  $K^-$ , the second for the  $\bar{K}_0$  at  $\rho_n = 1.5 \rho_p$  and  $\rho_p = 0$ .

the coupling of the antikaon to the  $\Lambda(1115)$  and  $\Sigma(1185)$  nucleon-hole states.

The non-trivial dynamics implied by the presence of the hyperon resonances reflects itself in a complicated behavior of the antikaon self energy,  $\Pi_{\bar{K}}(\omega, \vec{q}; \rho)$ . This is illustrated by the antikaon nuclear optical potential  $V_{\text{opt.}}(\vec{q}; \rho)$ , which may be defined by

$$2 E_K(\vec{q}) V_{\text{opt.}}(\vec{q}; \rho) = \Pi_{\bar{K}}(\omega = E_K(\vec{q}), \vec{q}; \rho), \quad E_K(\vec{q}) = \sqrt{m_K^2 + \vec{q}^2}. \quad (5.4)$$

In Fig. 9 the result for the optical potential is presented as a function of the antikaon momentum  $\vec{q}$  and the nuclear matter density. The real part of the optical potential exhibits rather moderate attraction of about 20 MeV at nuclear saturation density and  $\vec{q} = 0$  MeV. The attraction is further diminished and even turns into repulsion as the antikaon momentum increases. On the other hand the figure shows a rather strong absorptive part of the optical potential. This agrees qualitatively with computations based on self consistent s-wave dynamics<sup>8)</sup> but is in striking disagreement with mean-field calculations<sup>65)</sup> that predict considerable more attraction in the antikaon optical potential. The large attraction in the antikaon spectral function of Fig. 8 is consistent with the moderate attraction in the optical potential of Fig. 9. It merely reflects the strong energy dependence of the kaon self energy induced by the  $\Lambda(1405)$  and  $\Sigma(1385)$  resonances. Such important energy variations are missed in a mean-field approach. Hence, a proper treatment of the pertinent many-body effects is required.

In Fig. 10 the propagation properties of the  $\Lambda(1405)$  and  $\Sigma(1385)$  resonances

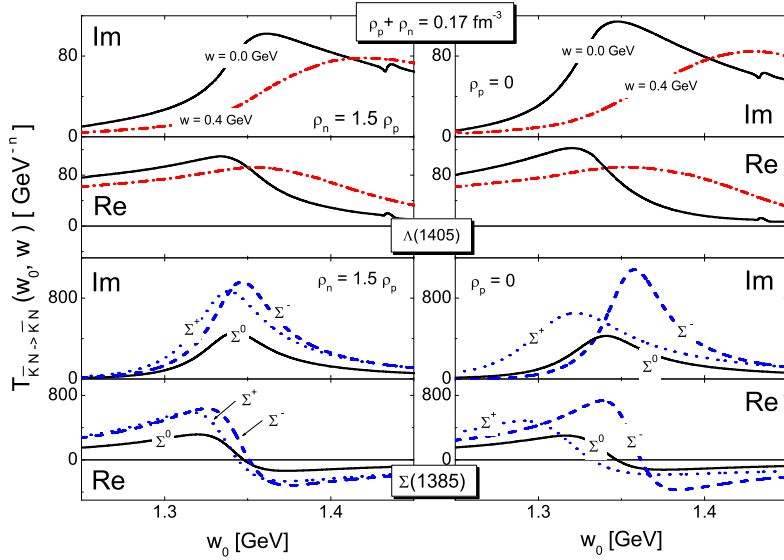


Fig. 12.  $\Lambda(1405)$  and  $\Sigma(1385)$  hyperon resonance propagators as a function of hyperon energy  $w_0$  and momentum  $\vec{w}$  for asymmetric nuclear matter. It is shown the s-wave  $K^- p \rightarrow K^- p$  (for  $\vec{w} = 0$  MeV and  $\vec{w} = 400$  MeV) and p-wave  $\bar{K}^0 n \rightarrow \bar{K}^0 n$ ,  $\bar{K}^0 p \rightarrow \bar{K}^0 p$  and  $K^- n \rightarrow K^- n$  reaction amplitudes (for  $\vec{w} = 0$  MeV) at  $\rho_n + \rho_p = 0.17$  fm $^{-3}$ .

as they move with finite three momentum  $\vec{w}$  in isospin symmetric nuclear matter are studied. The peak positions in the imaginary parts of the amplitudes follow in general the naive expectation  $\sqrt{(m_Y^*)^2 + \vec{w}^2}$  with the hyperon effective mass  $m_Y^*$  defined at  $\vec{w} = 0$ . However, a systematic increase of the decay widths as  $\vec{w}$  increases is observed. This is easily understood since the effective in-medium  $Y^* N \rightarrow Y^* N$  amplitude which is responsible for the broadening allows for additional inelasticity as the hyperon momentum  $\vec{w}$  increases. An interesting phenomenon illustrated in Fig. 10 is the in-medium induced mixing of partial wave amplitudes with different quantum numbers  $J^P$ . At vanishing three momentum of the meson-baryon state  $\vec{w} = 0$ , all partial-wave amplitudes decouple. In this case the system enjoys a three-dimensional rotational symmetry since there is no three-vector available to select a particular direction. However, once the meson-baryon pair is moving relative to the nuclear matter bulk with  $\vec{w} \neq 0$  there are two separate channels for a given isospin only. The system is invariant under a subgroup of rotations only, namely those for which the rotational vector is aligned with the hyperon momentum  $\vec{w}$ . The three-dimensional rotational symmetry is reduced and therefore the total angular momentum  $J$  is no longer a conserved quantum number. However, the total angular momentum projection onto the  $\vec{w}$  direction remains a conserved quantum number. The latter defines the helicity of a hypothetical s-channel particle exchange and therefore the in-medium scattering amplitudes decouple into an infinite tower of helicity amplitudes. Each helicity amplitude probes a well defined infinite set of partial wave amplitudes. For instance, in the helicity one-half space, all considered

partial wave amplitudes  $S_{I1}$ ,  $P_{I1}$ ,  $P_{I3}$  and  $D_{I3}$  couple for given isospin channel  $I$ . Note that reflection symmetry implies that only the absolute value of the helicity matters here. It is evident that all partial-wave amplitudes contribute to this channel simply because any state with a given angular momentum  $L$  has a component where  $\vec{L} \cdot \vec{w}$  vanishes and therefore the helicity is carried by the nucleon spin. In the second channel, the helicity three-half space, only the partial wave amplitudes  $P_{I3}$  and  $D_{I3}$  couple. In a computation that considered all partial waves the helicity three half term would require all partial wave amplitudes except the  $S_{I1}$  and  $P_{I1}$  waves with  $J = 1/2$ . The fact that the  $J = \frac{3}{2}$  amplitudes  $P_{I3}$  and  $D_{I3}$  affect both considered helicity spaces, is not surprising, because for those states one would expect the nuclear medium to lift the degeneracy of the four spin modes. This is completely analogous to the longitudinal and transverse modes of vector mesons, which bifurcate in nuclear matter.

The splitting of the four  $\Sigma(1385)$  modes is demonstrated in the left hand panel of Fig. 10. The helicity one and three half modes are shifted by about 5 MeV for  $\vec{w} = 600$  MeV. This is a small effect and therefore it is justified to neglect the coupling of the partial waves for that density to good accuracy. Indeed a run where all off diagonal loop functions that couple waves of different angular momentum or parity are set to zero gives results that are almost indistinguishable to those obtained in the full scheme. This is demonstrated by the dashed lines in the left hand panel of Fig. 10. At  $\vec{w} = 0$  the results of the two computations, dashed and solid lines are quite close. This finding has a simple interpretation. One expects sizeable effects from the in-medium mixing of the partial-wave amplitudes only if two partial wave amplitudes that mix show both significant strength at a given energy  $w_0$ . This is not the case here. The dominant partial waves  $S_{01}$  and  $P_{13}$  decouple because they carry different total isospin. Therefore it is natural to obtain small mixing effects.

A discussion of results<sup>6),7),12)</sup> obtained for asymmetric nuclear matter follows. Two cases are considered here both with  $\rho_n + \rho_p = 0.17$  fm<sup>-3</sup>. In Fig. 11 results for  $\rho_n = 1.5 \rho_p$ , which corresponds to the condition met in the interior of lead, and for  $\rho_p = 0$ , which describes neutron matter, are shown. The asymmetry breaks up the isospin doublet ( $K^-, \bar{K}_0$ ) leading to distinct spectral functions for the charged and neutral antikaons. In both cases a significant effect from the self consistency is found at small antikaon momenta. This is illustrated by comparing the entries of Fig. 11 labeled with 'Tρ' and 'SC'. Whereas the effect of the asymmetry is surprisingly small for the lead scenario, the spectral functions of the charged and neutral antikaons differ strongly in neutron matter with  $\rho_p = 0$ . In Fig. 12 the corresponding properties of the hyperon resonances are shown. Again, like one observed for the isospin doublet ( $K^-, \bar{K}^0$ ) the isospin asymmetry of the matter breaks up the isospin triplet state  $\Sigma(1385)$  introducing a medium-induced splitting pattern. The  $\Lambda(1405)$  resonance is presented in terms of the in-medium  $K^- p \rightarrow K^- p$  s-wave amplitude, the neutral and charged  $\Sigma(1385)$  states by p-wave amplitudes  $\bar{K}^0 n \rightarrow \bar{K}^0 n$ ,  $\bar{K}^0 p \rightarrow \bar{K}^0 p$  and  $K^- n \rightarrow K^- n$ . In free space the latter amplitudes are determined by the isospin one amplitude in case of the charged hyperon states but by the mean of the two isospin amplitudes in case of the neutral hyperon state. Thus, the isospin one component, the  $\Sigma(1385)$  couples to in free space, is smaller by a factor of two for the neutral amplitude

$\bar{K}^0 n \rightarrow \bar{K}^0 n$  as compared to the amplitudes describing the charged hyperon states. This reflects itself in amplitudes for the  $\Sigma^0(1385)$  in Fig. 12 that are typically smaller by a factor two as compared to the amplitudes of the  $\Sigma^\pm(1385)$ . Whereas the  $\Lambda(1405)$  resonance is not affected much by the asymmetry, the splitting of the three  $\Sigma(1385)$  states shows a strong dependence on the asymmetry. For neutron matter with  $\rho_n = 0.17 \text{ fm}^{-3}$  a mass difference of about 30 MeV for the charged states is found.

## §6. Summary

In this talk we reported on recent progress in the understanding of baryon resonances based on chiral-coupled channel dynamics. An introduction to an effective field theory formulation of chiral coupled-channel dynamics was given. Leading order results predict the existence of s- and d-wave baryon resonances with a spectrum remarkably close to the empirical pattern without any adjustable parameters. The formation of resonances is a consequence of the chiral  $SU(3)$  symmetry of QCD, i.e. in an effective field theory, that was based on the chiral  $SU(2)$  symmetry only, no resonances would be formed. Realistic scattering amplitudes that are consistent with empirical differential cross sections can be obtained after including chiral corrections terms systematically.

As a further application of chiral coupled-channel dynamics results for antikaon and hyperon resonance propagation in cold nuclear matter were presented. Based on scattering amplitudes obtained within the chiral coupled-channel effective field theory a self consistent density summation scheme can be performed that respects covariance manifestly. As a consequence the spectral function of the antikaon shows a strong momentum and density dependence in isospin symmetric and asymmetric matter. For the  $\Lambda(1405)$  and  $\Sigma(1385)$  resonances attractive mass shifts are predicted.

## References

- 1) A.D. Martin, Nucl. Phys. **B 179** (1981) 33.
- 2) C.D. Dover, J. Hüfner and R.H. Lemmer, Ann. Phys. **66** (1971) 248.
- 3) M. Lutz, A. Steiner and W. Weise, Nucl. Phys. **A 574** (1994) 755.
- 4) M. Lutz, Phys. Lett. **B 426** (1998) 12; M.F.M. Lutz, in *Proc. Workshop on Astro-Hadron Physics*, Seoul, Korea, October, 1997, World Scientific 1999.
- 5) M.F.M. Lutz and E.E. Kolomeitsev, Nucl. Phys. **A 700** (2002) 193.
- 6) M.F.M. Lutz and C.L. Korpa, Nucl. Phys. **A 700** (2002) 309.
- 7) C.L. Korpa and M.F.M. Lutz, Heavy Ion Phys. **17** (2003) 341.
- 8) M.F.M. Lutz and W. Florkowski, Act. Phys. Pol. **31** (2000) 2567.
- 9) A. Cieply, E. Friedman, A. Gal and J. Mares, Nucl. Phys. **A 696** (2001) 173.
- 10) M.F.M. Lutz und E.E. Kolomeitsev, Found. Phys. **31** (2001) 1671.
- 11) M.F.M. Lutz, Gy. Wolf and B. Friman, Nucl. Phys. **A 706** (2002) 431.
- 12) M.F.M. Lutz, GSI-Habil-2002-1.
- 13) C. García-Recio, M.F.M. Lutz and J. Nieves, Phys. Lett. **B 582** (2004) 49.
- 14) E.E. Kolomeitsev and M.F.M. Lutz, Phys. Lett. **B 585** (2004) 243.
- 15) M.F.M. Lutz and E.E. Kolomeitsev, Nucl. Phys. **A 730** (2004) 392.
- 16) E.E. Kolomeitsev and M.F.M. Lutz, Phys. Lett. **B 582** (2004) 39.
- 17) M.F.M. Lutz and E.E. Kolomeitsev, Nucl. Phys. **A 730** (2004) 110.
- 18) J. Hofmann and M.F.M. Lutz, Nucl. Phys. **A 733** (2004) 142.
- 19) H.W. Wyld, Phys. Rev. **155** (1967) 1649.

- 20) R.H. Dalitz, T.C. Wong and G. Rajasekaran, Phys. Rev. **153** (1967) 1617.
- 21) J.S. Ball and W.R. Frazer, Phys. Rev. Lett. **7** (1961) 204.
- 22) G. Rajasekaran, Phys. Rev. **5** (1972) 610.
- 23) R.K. Logan and H.W. Wyld, Phys. Rev. **158** (1967) 1467.
- 24) P.B. Siegel and W. Weise, Phys. Rev. **C 38** (1988) 2221.
- 25) M.F.M. Lutz and E. E. Kolomeitsev, Proc. of Int. Workshop XXVIII on Gross Properties of Nuclei and Nuclear Excitations, Hirschegg, Austria, January 16-22, 2000.
- 26) A. Krause, Helv. Phys. Acta **63** (1990) 3.
- 27) S. Weinberg, *The quantum theory of fields*, Vol. II, University Press, Cambridge (1996).
- 28) M.F.M. Lutz, Nucl. Phys. **677** (2000) 241.
- 29) J. Nieves and E. Ruiz Arriola, Nucl. Phys. **A 679** (2000) 57.
- 30) S. Weinberg, Phys. Rev. Lett. **17** (1966) 616;  
Y. Tomozawa, Nuov. Cim. **A 46** (1966) 707.
- 31) N. Kaiser, P.B. Siegel and W. Weise, Nucl. Phys. **A 594** (1995) 325.
- 32) J. Nieves and E. Ruiz Arriola, Phys. Rev. **D 63**, (2001) 076001.
- 33) C. García-Recio, J. Nieves, E. Ruiz Arriola and M. J. Vicente-Vacas, Phys. Rev. **D 67** (2003) 076009.
- 34) A. Ramos, E. Oset and C. Bennhold, Phys. Rev. Lett. **89** (2002) 252001.
- 35) E. Oset, A. Ramos, C. Bennhold, Phys. Lett. **B 527** (2002) 99.
- 36) D. Jido et al., Nucl. Phys. **A 725** (2003) 181.
- 37) C.L. Schat, J.L. Goity and N.N. Scoccola, Phys. Rev. Lett. **88** (2002) 102002.
- 38) F. Karsch, Nucl. Phys. B (Proc. Suppl.), 83-84 (2000) 14.
- 39) G. Boyd, et al. Phys. Lett. **B 349** (1995) 170.
- 40) T. Hatsuda, hep-ph/0104139.
- 41) D. G. Richards, Proc. of 'NSTAR 2002', Pittsburgh, October 2002, and references therein.
- 42) G. Höhler,  $\pi N$  NewsLetter **9** (1993) 1.
- 43) B.R. Martin and M. Sakit, Phys. Rev. **183** (1969) 1352.
- 44) J.K. Kim, Phys. Rev. Lett. **14** (1965) 29.
- 45) M. Sakit et al., Phys. Rev. **139** (1965) B179.
- 46) G.P. Gopal et al. Nucl. Phys. **119** (1977) 362.
- 47) G. C. Oades, in Proc. of *Int. Workshop on Low and Intermediate-Energy Kaon-Nucleon Physics*, Rome, Italy, 24-28 March 1980, (eds. E. Ferrari, G. Violini), D. Reidel Publishing, Dordrecht (1980).
- 48) A. Müller-Groling, K. Holinde and J. Speth, Nucl. Phys. **A 513** (1990) 557.
- 49) R.H. Dalitz and A. Deloff, J. Phys. **G 17** (1991) 289.
- 50) N. Kaiser, P.B. Siegel and W. Weise, Nucl. Phys. **A 594** (1995) 325;  
N. Kaiser, T. Waas and W. Weise, Nucl. Phys. **A 612** (1997) 297.
- 51) E. Oset and A. Ramos, Nucl. Phys. **A 635** (1998) 99.
- 52) T.S. Mast et al., Phys. Rev. **D 11** (1975) 3078.
- 53) R.O. Bangerter et al., Phys. Rev. **D 23** (1981) 1484.
- 54) D.B. Kaplan and A.E. Nelson, Phys. Lett. **B 175** (1986) 57.
- 55) G.E. Brown and H.A. Bethe, Astrophys. Jour. **423** (1994) 659.
- 56) G.Q. Li, C.-H.Lee, G.E. Brown, Phys. Rev. Lett. **79** (1997) 5214; Nucl. Phys. **A 625** (1997) 372.
- 57) T. Muto and T. Tatsumi, Phys. Lett. **B 283** (1992) 165; T. Muto, Nucl. Phys. **A 697** (2002) 225.
- 58) E.E. Kolomeitsev and D.N. Voskresensky, Phys. Rev. **C 68** (2003) 015803.
- 59) A. Dote, H. Horiuchi, Y. Akaishi and T. Yamazaki, nucl-th/0207085 , nucl-th/0309062;
- 60) F. Laue, Ch. Sturm et al., Phys. Rev. Lett. **82** (1999) 1640.
- 61) E.E. Kolomeitsev, D.N. Voskresensky and B. Kämpfer, Nucl. Phys. **A 588** (1995) 889.
- 62) V. Koch, Phys. Lett. **B 337** (1994) 7.
- 63) A. Ramos and E. Oset, Nucl. Phys. **A 671** (2000) 481.
- 64) L. Tolos, A. Ramos, A. Polls and T.S. Kuo, Nucl. Phys. **A 690** (2001) 547.
- 65) J. Schaffner, J. Bondorf and I.N. Mishustin, Nucl. Phys. **A 625** (1997) 325.